Available online at www.sciencedirect.com
SCIENCE DIRECT®
Journal of Nuclear Materials 318 (2003) 234–240
journal of nuclear materials
www.elsevier.com/locate/jnucmat

The effect of cascade induced gas resolution on bubble formation in metals

H. Trinkaus *

ESS-Projekt, Forschungszentrum Jülich, D-52425 Jülich, Germany

Abstract

Transmission electron microscopy observations of bubble structures formed during He ion implantation by accelerators indicate that bubbles nucleate at very low He concentrations (<10 appm) and displacement doses ($<10^{-3}$ dpa), depending on temperature, and grow with increasing He concentration and dose at almost constant density after the nucleation peak. At intermediate temperatures, experimental data for higher doses indicate that bubble densities start (already at doses well below 1 dpa) to increase almost linearly with He concentration and dose, now at essentially constant bubble size. In the present contribution it is shown that this high dose feature of bubble formation may be attributed to the nucleation of bubbles under the internal He generation resulting from the resolution of He atoms from existing bubbles by displacement cascades. A simple analytical model, assuming that a certain fraction of He atoms in a bubble is resolved per dpa and that di-He clusters form a stable bubble nucleus, is presented, yielding for high doses a linear increase of the bubble density with dose at constant bubble size. This model is used to discuss the contribution of He bubbles to the hardening of metals under irradiation associated with He production, particularly its dependence on He concentration, displacement dose, and He-to-dpa ratio.

1. Introduction

Macroscopic radiation damage effects in structural components of nuclear devices are the consequence of two fundamentally different types of interactions between the projectile particles of the irradiation and the atoms of the irradiated material: atomic displacements resulting in vacancy and self-interstitial type lattice defects, and nuclear reactions creating foreign elements [1]. The creation of helium atoms in metals is considered with particular concern since their precipitation into bubbles can substantially contribute to radiation embrittlement. At high (homologous) temperatures, $T \geqslant 0.5T_m$ (T_m: melting temperature), drastic embrittlement of metals due to helium bubble formation at grain boundaries has been found to occur even at very low overall helium concentrations [1–3]. At lower temperatures, $0.2T_m < T < 0.5T_m$, a significant contribution of helium to embrittlement seems to require helium concentrations of about 1 at.% [4–7].

Most of the knowledge on the kinetics of helium bubble formation in metals, particularly at elevated temperatures, $T > 0.5T_m$, is due to transmission electron microscopy (TEM) of bubble structures formed during He ion implantation by accelerators. In such experiments, bubbles seem to nucleate at very low He concentrations (<10 appm) and displacement doses ($<10^{-3}$ dpa), depending on temperature, and seem to grow with increasing implanted He concentration and dose at almost constant density after the early nucleation peak [2]. This behaviour has been interpreted as a 'self-limitation' of bubble nucleation due to the reduction of the atomic He concentration in 'solution' by the increasing absorption of He atoms by the increasing density and size of bubbles [3,8,9].

This feature and its interpretation holds, however, only for low total (implanted or generated) He concentration and/or low displacement dose where the dynamic re-solution of He atoms from existing bubbles by displacement cascades is negligible compared to the

* Tel.: +49-2461 616460; fax: +49-2461 612620.
E-mail address: h.trinkaus@fz-juelich.de (H. Trinkaus).

0022-3115/03/$ - see front matter © 2003 Elsevier Science B.V. All rights reserved.
doi:10.1016/S0022-3115(03)00103-X

implantation or generation of further He atoms. At higher He concentration/dose, He resolution from existing bubbles will lead to the nucleation of a secondary generation of bubbles. This effect was first discussed by Nelson for the case of He resolution from bubbles by fission fragments in UO_2 [10]. Later, Chou and Ghoniem treated the related problem of cascade-induced dissolution of solid precipitates [11,12], and Ghoniem presented a model for He-resolution and re-nucleation of bubbles in metals under cascade damage conditions [13].

For metals implanted with He at intermediate temperatures, $0.2 < T/T_m < 0.5$, there is now convincing experimental evidence for the nucleation of secondary and higher order generations of bubbles from He atoms resolved form existing primary bubbles by displacement cascades. A most striking example for this effect is the formation of halos of secondary bubbles around primary ones in a ferritic model alloy pre-implanted with He at elevated temperature and subsequently irradiated with Fe ions at lower temperature [14] (Fig. 1). Another example is the observation of differences in bubble densities for different types of martensitic/ferritic steels irradiated under different conditions, which have been recently attributed to different properties of He atoms and He bubbles in Fe-based alloys of different composition [15]. Inspection of the experimental data shows, however, that higher bubble densities are consistently correlated with higher applied displacement doses, suggesting that increased bubble densities are, in fact, due to bubble nucleation from He atoms resolved from existing bubbles by displacement cascades rather than due to differences between alloys [16]. Thus, there is no doubt that irradiation results in the resolution of He atoms from existing bubbles, inducing the nucleation of later generations of bubbles.

In the present contribution, a simple model is presented, allowing a fully analytical description of gas resolution from existing bubbles by displacement cascades and bubble formation under the related internal He generation. The implications of these effects for hardening and embrittlement of metals under He generation and displacement damage are discussed.

2. Modeling cascade induced gas resolution from bubbles

In multi-component/multi-phase systems, displacement cascades cause substantial atomic re-ordering, a phenomenon called 'cascade mixing' (or 'ion-beam mixing' in ion-beam technologies). For the present purpose, the two most important results of detailed experimental studies of ion-beam mixing in many metallic systems at low ambient temperatures (where even radiation enhanced diffusion is negligible) are [17]

1. the 'mixing efficiency' is significantly higher than expected according to ballistic (collisional) models,
2. no correlation seems to exist between the mixing efficiency and the atomic masses of the components involved.

These findings have been attributed to atomic diffusion during the thermal spike phase of displacement cascades [17].

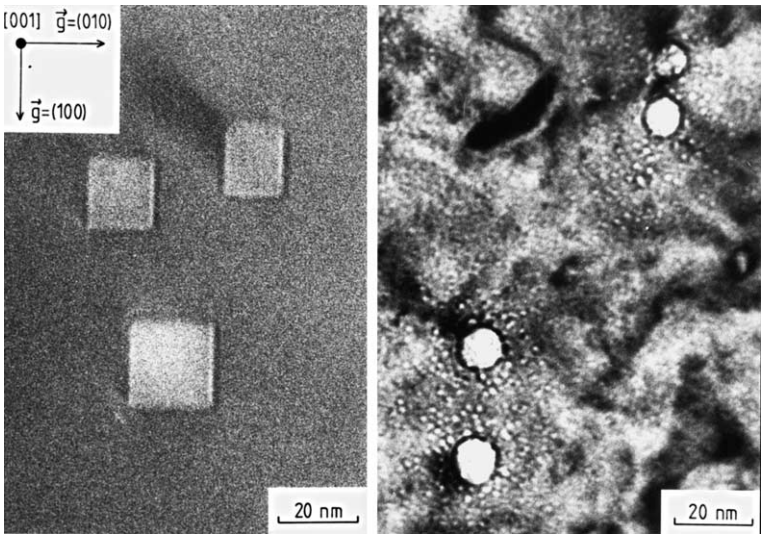

Fig. 1. Bubbles in Fe–12%Cr (a) after 100 keV He^+ implantation to 600 appm He at 973 K, (b) after 100 keV He^+ implantation to 600 appm He at 973 K and subsequent 300 keV Fe^+ irradiation to 30 dpa at 573 K [14]. Notice the halos of small bubbles around the large parent bubbles, obviously formed by He atoms resolved from the parent bubbles.

To my knowledge, the effect of cascades on gas bubbles has not been studied systematically so far. At a first view, one is inclined to expect lower mixing efficiencies compared to solid-in-solid systems, primarily because of larger differences in atomic masses (for He-bubbles and even more for H-bubbles) and densities of gas and matrix atoms; but, according to point (2) mentioned above, differences in atomic masses do not significantly affect mixing efficiencies, and, at the intermediate temperatures of interest here ($0.2T_m < T < 0.5T_m$), densities of gas atoms in small bubbles do not differ significantly from densities of matrix atoms [18]. Thus, effects of cascades on gas bubbles may be expected to be similar to those on solid-in-solid systems.

There is, however, another difference to be considered here: the driving force for an annealing of a disintegrated interface (surface) during the late spike and in the post-spike phases is much stronger for bubbles than for solid precipitates because of a substantially higher specific interface (surface) free energy, an effect which may be expected to reduce the effective mixing efficiency. Nevertheless, the shrinkage of bubbles and the size of the halos around the bubbles in the structure shown in Fig. 1 [14] indicates a value of the order of 10 Å^5/eV for the mixing efficiency corresponding to an effective mixing diffusion constant of the order of 1 K nm^2 (K, displacement rate) for He in steels [16], quite comparable to the corresponding values for solid-in-solid systems [17].

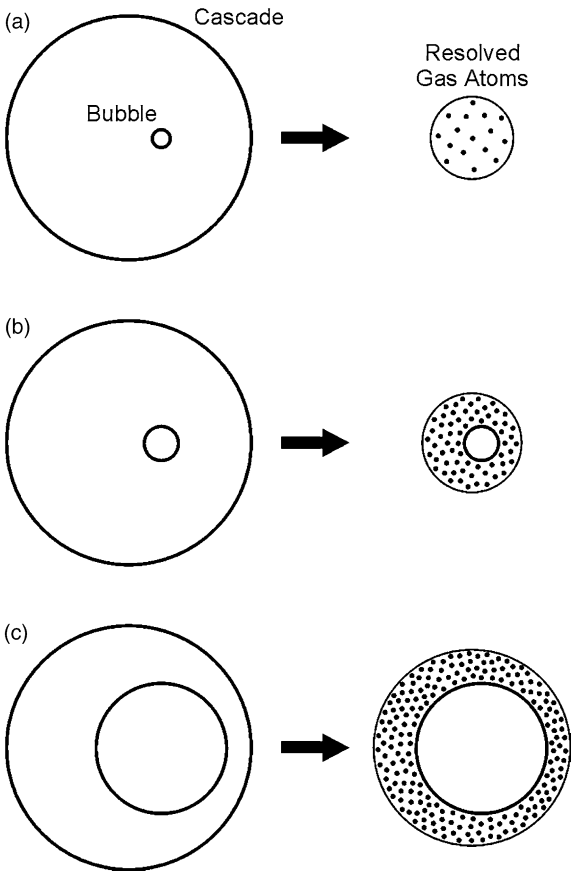

Fig. 2. Schematic illustration of the dependence of cascade-induced gas resolution and escape from a bubble on bubble size in relation to mixing range of the gas atoms. (a) Small bubble nucleus (gas-vacancy cluster): complete dissolution, all gas atoms are able to escape; (b) sub-nm-sized bubble: a substantial fraction of the gas atoms are resolved and are able to escape; (c) large bubble (> a few nm): only gas atoms close to bubble boundary are resolved, most of which return to their mother bubble.

In the present context, special interest is to be focused on the cascade-induced resolution of gas (He) atoms from existing bubbles and their escape from their parent bubbles by radiation enhanced diffusion at intermediate temperatures where the latter is dominant ($0.2T_m < T < 0.5T_m$). Cascade-induced gas resolution and escape from existing bubbles depends on bubble size in relation to the gas atom diffusion range reached in the thermal spike phase of a cascade. As indicated previously [10–13], the following cases may be distinguished (Fig. 2):

(1) Atomically small bubble nuclei (He-vacancy clusters) may be expected to become completely dissolved by the impact of one cascade (Fig. 2(a)).
(2) Small nm-sized bubbles will be completely or partially dissolved in the hot spike phase and, from this, one (or a few) dominant bubble(s) will be re-nucleated in the centre of the cascade, or the possibly remaining residue of the original bubble will be partially re-established in the cooling phase of the cascade. As long as the final size of the central bubble is smaller (<1 nm) than the cascade mixing range (up to a few nm) (Fig. 2(b)), a substantial fraction of the resolved gas atoms (and small bubble nuclei) in its surroundings will be able to escape at temperatures where the latter are mobile.
(3) For larger bubbles (> a few nm), only gas atoms close to their boundary will be affected by the impact of a cascade and most of the resolved gas atoms will return to their mother bubble (Fig. 2(c)).

In the following, the kinetics of bubble formation at intermediate temperatures ($0.2T_m < T < 0.5T_m$) will be considered where, on the one hand, gas atoms are mobile under irradiation, and, on the other hand, bubble sizes remain smaller than the cascade mixing range at doses of interest (case b). Assuming that, within this size range, a certain fraction of the gas atoms, contained in a bubble before a cascade impact, is able to escape after the impact, the rate of the secondary gas production associated with cascade induced gas resolution may be written as

$$P^{(2)} = \kappa K \hat{c}, \tag{1}$$

where κ is a parameter characterising the resolution efficiency, K is the displacement rate, and $\hat{c}$ is the part of the atomic gas concentration accumulated in bubbles. The resolution parameter κ is expected to depend on the average cascade structure, i.e. on the recoil energy spectrum, and, according to the above described scenario, also on the average bubble size [13]. For bubble sizes in the range of case b considered here, this size dependence may be neglected. The mixing efficiency of about 10 Å^5/eV estimated from the structure shown in Fig. 1 [14] indicates values $\kappa > 1$ ($\kappa \approx 3$) [16], i.e. values larger than deduced [12,13] or assumed [9] previously ($0.1 \leqslant \kappa \leqslant 1$). Unfortunately, to my knowledge, no other experiments or computer simulations are presently available for getting more information on relevant cascade resolution parameters such as κ.

The secondary gas production associated with cascade induced gas resolution becomes dominant over the primary one, $P^{(2)} > P^{(1)}$, only at a dose level where most of the gas atoms produced are accumulated in bubbles, i.e. where $\hat{c} \approx c = P^{(1)}t$ (c: total atomic gas concentration produced during time t). Using this in Eq. (1), one finds that $P^{(2)} > P^{(1)}$ applies at displacement doses $Kt > 1/\kappa$, i.e. even below 1 dpa for $\kappa > 1$.

3. Modeling bubble formation

The following considerations are devoted to the kinetics of bubble formation at intermediate temperatures ($0.2T_m < T < 0.5T_m$) where, on the one hand, gas atoms are mobile under irradiation, and, on the other, once formed bubble nuclei are thermally stable. The simplest assumption for this temperature range is that already two gas atoms form a stable bubble nucleus [19]. In this 'di-atomic nucleation' model discussed in detail in the 1980s [3,8,9], the rate equations for the evolution of the concentration of mobile gas atoms, $\check{c}$, and the number density of bubbles, N, may be written as

$$\mathrm{d}\check{c}/\mathrm{d}t = P - 2aD\check{c}^2 - 4\pi RD\check{c}N, \tag{2a}$$

$$\mathrm{d}N/\mathrm{d}t = a\check{c}^2, \tag{2b}$$

where $P = P^{(1)} + P^{(2)}$ is the total (primary plus secondary) gas production rate, $a = 8\pi r_0/\Omega \approx 10^{21}$ m^{-2} ($r_0 \approx 0.5$ nm, clustering radius; $\Omega \approx 10^{-29}$ m^3, volume per matrix atom) is a geometrical factor characterising the efficiency of gas atom clustering, D is the gas atom diffusivity and $R \geqslant r_0$ is the average radius of the evolving bubbles increasing continuously upon gas atom absorption. Binary defect-reaction equations of the form of Eqs. (2a,2b) may be assumed to be applicable at moderate total gas concentrations (<a few at.%) and bubble number densities (<10^{26} m^{-3}).

The evolution of the bubble structure passes several stages characterised by the dominance of certain combinations of terms in Eq. (1). The evolution at low gas concentrations/displacement doses where $P^{(2)} \ll P^{(1)}$ has been discussed previously in some detail [3,8,9]. It suffices therefore here to briefly review the main features of this low dose evolution.

3.1. Primary bubble nucleation

At constant primary gas production rate $P^{(1)}$, the initially increasing gas atom concentration $\check{c}$ and the associated nucleation rate surpass maxima, $\mathrm{d}\check{c}/\mathrm{d}t = 0$, $\mathrm{d}^2N/\mathrm{d}t^2 = 0$, when the 2nd and 3rd terms in Eq. (2a), i.e. the number densities of gas atoms and bubble nuclei, become comparable, meaning that in this stage a newly created gas atom is as likely to reach an existing nucleus as to meet another gas atom. After this nucleation peak, the gas atom concentration and the nucleation rate decrease continuously due to the increasing absorption of gas atoms by bubbles of increasing density and size. The density of bubble nuclei at the end of the thus 'self-limited' early nucleation phase is some multiple (two to three times) of that at the time of maximum nucleation rate. The condition that the nucleation and absorption (the 2nd and 3rd) terms in Eq. (2a) are comparable at the nucleation peak, where $\mathrm{d}\check{c}/\mathrm{d}t = 0$, yields, with $R \approx r_0$, an estimate for the bubble number density nucleated in the primary nucleation phase [3,8,9]

$$N \approx (P^{(1)}/\pi r_0 D\Omega)^{1/2} \text{ at } c \approx 2(\Omega P^{(1)}/r_0 D)^{1/2}. \tag{3}$$

As long as $P^{(2)} \ll P^{(1)}$, the bubble evolution beyond the nucleation phase is dominated by bubble growth due to the absorption of newly produced gas atoms. In this growth phase, the terms $\mathrm{d}\check{c}/\mathrm{d}t$ and $2aD\check{c}^2$ may be neglected in Eq. (2a), but, according to Eq. (2b), under this quasi-steady-state condition some bubble nucleation takes place at decreasing rate. The fact that, in this phase, most of the gas atoms produced are accumulated in bubbles, can be used to express the average radius, $R(t)$, by the number density, $N(t)$, of the bubbles and the total He concentration c (see below).

According to Eq. (3), the temperature dependence of the bubble density nucleated in the primary nucleation phase is characterised by an apparent activation energy E_a, equal to (minus) half of that of D. In the temperature range considered here, $0.2T_m < T < 0.5T_m$, gas atom (He) diffusion under irradiation is most likely controlled by the replacement of gas atoms from substitutional sites by self-interstitial atoms (replacement mechanism). In this case, D is equal to the vacancy diffusion coefficient D_v [8,9,20], and E_a is consequently half of the vacancy migration energy, $E_a = E_v^m/2$. The corresponding function for N according to Eq. (3) is in order of magnitude agreement with bubble densities observed in He

implantation experiments, including its relatively weak temperature dependence in this temperature range [9]. Experimental and theoretical bubble densities between 10^{21} and 10^{23} m^{-3} indicate that primary bubble nucleation occurs at very low He concentrations around and below 1 appm (and correspondingly low displacement doses).

It is noted here that the possibilities of replacement of more than one gas atoms from a substitutional site by one self-interstitial atom and the migration and coalescence of small bubbles result in reduced bubble densities compared to Eq. (3), but, otherwise, do not change the general conclusions concerning the nucleation phase and the dependence of the nucleated bubble densities on the main parameters P and $D(T)$ [9].

3.2. Secondary bubble nucleation

At significant displacement doses $Kt \approx 1/\kappa$, the secondary gas production associated with cascade induced gas resolution becomes important, $P^{(2)} \approx P^{(1)}$. In this phase, the fact that most of the gas atoms produced are accumulated in bubbles, may be used to express $\hat{c}$ in Eq. (1) by $P^{(1)}t$ and R in Eq. (2a) by N

$$P^{(2)} \approx \kappa K P^{(1)} t, \tag{4}$$

$$(4\pi/3)R^3 N \approx P^{(1)} t (v/\Omega), \tag{5}$$

where $v \approx \Omega$ [18] is the volume per gas atom in bubbles. Assuming that this remains constant during bubble evolution and using in addition that, in this medium to high dose phase, $\mathrm{d}\check{c}/\mathrm{d}t$ (quasi-steady-state) and $2aD\check{c}^2$ (growth dominant) may be neglected in Eq. (2a), $\check{c}$ in Eq. (2b) can be expressed by N. Elementary integration yields then $N(t)$ and, with aid of Eq. (5), $R(t)$. The result, valid beyond the primary nucleation peak, is shown in Fig. 3, where the bubble density, $N(t)$, and the average number of gas atoms per bubble, $n_g = (4\pi/3)R^3/v = P^{(1)}t/(\Omega N)$, normalised to their values at $\kappa Kt = 1$, are plotted vs. the 'effective dose' κKt. For doses $\kappa Kt \ll 1$, $N(t)$ increases only very weakly ($N \sim t^{1/7}$) while n_g increases almost linearly with dose ($n_g \sim t^{6/7}, R \sim t^{2/7}$), whereas for $\kappa Kt \gg 1$, $N(t)$ increases linearly while n_g converges to an asymptotically constant value. Here, only the asymptotic high dose behaviour is quoted:

$$N = (\Omega/48\pi^2 v)^{2/7} (aP^{(1)}/\Omega D)^{3/7} (P^{(1)}/\kappa K)^{1/7} \kappa K t, \tag{6a}$$

$$R = [27 v^3 D P^{(1)}/4\pi\Omega^2 a \kappa^2 K^2]^{1/7}. \tag{6b}$$

According to Eqs. (6a) and (6b), in this high dose range, bubble density and size do not only depend on the primary gas production rate, $P^{(1)}$, but even stronger on the displacement rate K. Both depend, via $D(T)$, only weakly on temperature. For $K = 100P^{(1)} = 10^{-6}$ s^{-1}, typical for He implantation experiments (and $\kappa = 3$, $\Omega = 10^{-29}$ m^3, $a = 10^{21}$ m^{-2}, $D = D_v = 10^{-5}\exp(-6T_m/T)$ m^{-2}) Eqs. (6a) and (6b) yield at $Kt = 1$ dpa: $N = 1.2 \times 10^{25}$ m^{-3}, $R = 0.6$ nm and $N = 5 \times 10^{21}$ m^{-3}, $R = 7.5$ nm for $T = 0.2T_m$ and $0.5T_m$, respectively.

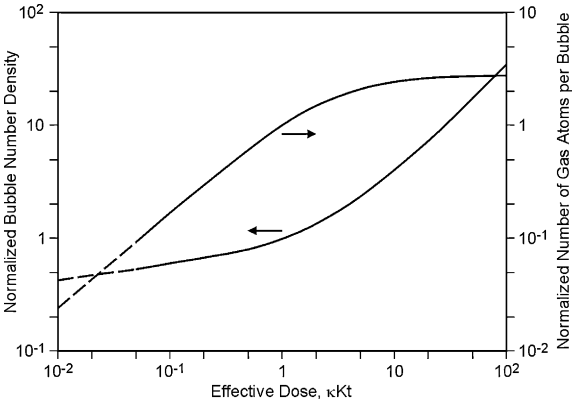

Fig. 3. Bubble density and average number of gas atoms per bubble, normalised to their values at $\kappa Kt = 1$, vs. the 'effective dose' κKt. For $\kappa Kt \ll 1$ (left), the lines are broken to indicate that they are valid only beyond the primary nucleation peak.

From these values, it becomes clear that $0.2T_m$ and $0.5T_m$ mark the lower and upper temperature limits of the approximations used here. Below $0.2T_m$ (annealing stage III), the mechanism of gas (He) diffusion changes from the replacement mechanism to the cascade mixing mechanism [20], primary and secondary bubble nucleation become indiscernible and bubble nuclei formed do not exceed sizes of atomic scale (He-vacancy clusters containing up to a few tens of He atoms), unless bubble migration and coalescence occur at high gas concentrations. Above $T_m/2$ (annealing stage VI), gas resolution becomes increasingly inefficient because of increasing reabsorption of resolved gas atoms for increasing bubble sizes (case c in Section 2, Fig. 2(c)), whereas thermal dissociation of gas atoms from bubbles becomes increasingly important.

It must be emphasised here, that, at all temperatures, Eqs. (6a) and (6b) represent upper and lower bound estimates for the bubble density and size, respectively. The replacement of more than one gas atom from a substitutional site by one self-interstitial atom, for instance, would result in a reduction of the bubble density and increase the bubble size compared to Eqs. (6a) and (6b). At high gas concentrations (around and above 1 at.%), the bubble density is expected to be limited by inter- and/or intra-cascade bubble migration and coalescence.

4. Implications for hardening

An important consequence of damage accumulation in metals under energetic neutron, proton or He

irradiation is hardening (increase in yield stress, $\Delta\sigma_y$) and embrittlement (decrease of the strain to failure). There are two types of microstructural components contributing to hardening [21]:

(1) displacement damage in the form of defect clusters, dislocation loops and the thereof evolving dislocation network, and
(2) bubbles, primarily filled with He.

Mechanical tests on austenitic and martensitic steels irradiated at or somewhat above room temperature indicate that

(1) the hardening increment per dpa decreases with increasing displacement dose and tends to saturate above about 1 dpa, and
(2) the contribution of bubbles to hardening is negligible at low He concentrations and becomes, after He implantation, significant only above a critical He concentration around 1 at.% [4–7].

In discussing the contribution of He to hardening the 'dispersed barrier hardening model' for discrete obstacles is used where the increase in the yield stress behaves as [21]

$$\Delta\sigma_y \sim \sqrt{(RN)}. \tag{7}$$

According to the above described model, the contribution of bubbles to hardening described by the function $\sqrt{(RN)}$ increases only weakly ($\sim t^{3/14}$) with He concentration/dose, certainly much weaker than the contribution of displacement damage, between the primary nucleation peak, occurring at low He concentrations, and the dose $Kt = 1/\kappa$, where cascade induced He resolution from bubbles becomes significant. This weak dependence changes at higher doses, $\kappa Kt > 1$, to a dependence stronger than that due to displacement damage. In this dose range, equations (6a,6b) yield the scaling behaviour

$$\begin{aligned}\Delta\sigma_y &\sim [P^{(1)5}/(\kappa K)^3 D^2]^{1/14}\sqrt{(\kappa K t)} \\ &\sim [(\kappa K)^4/P^{(1)2}D^2]^{1/14}\sqrt{(c)}.\end{aligned} \tag{8}$$

According to Eq. (8), the contribution of bubbles to hardening may be written to increase with the square root of the He concentration or with the square root of the displacement dose, with factors depending, in opposite directions, on the He-to-dpa ratio, and in addition, on the ratio of one of the rates to the He diffusion coefficient $D(T)$. To reach a certain ('critical') level of hardening due to bubbles at a given temperature (given $D(T)$), a certain minimum ('critical') He concentration or displacement dose is required, increasing with $[P^{(1)2}/(\kappa K)^4)]^{1/7}$ and $[(\kappa K)^3/P^{(1)5}]^{1/7}$ (increasing and decreasing with increasing He-to-dpa ratio), respectively.

In Table 1, an attempt is made to extrapolate the known critical He concentration of 1 at.% and critical dose of 1 dpa, respectively, for a significant contribution of bubbles to hardening after He implantation [4–7] to the irradiation conditions of fast fission reactors, fusion reactors, and spallation neutron sources assuming that the value of the resolution parameter κ is the same in all cases. Since κ is certainly larger under pronounced cascade damage conditions than under He implantation conditions, only upper bound values for critical He concentrations and doses can be given for the three cases considered, indicated by the sign $\leqslant$ in Table 1. It becomes, however clear from Table 1 that the critical He concentrations and displacement doses in reactors and spallation neutron sources are lower and higher, respectively, than in the case of He implantation, respectively. This general statement which is found to be rather insensitive against modifications of the model [16], should be checked by mechanical tests on samples implanted with He to different levels between 0.05 and 1 at.% and irradiated (simultaneously) with self-ions or (subsequently) with fast neutrons up to high displacement doses.

It must, however, be emphasized here that a quantitative application of the 'dispersed barrier hardening

Table 1
Extrapolation of critical He concentration and displacement dose for a significant contribution of bubbles to hardening after He implantation to the irradiation conditions of fast fission reactors, fusion reactors, and spallation neutron sources. The sign $\leqslant$ is introduced to indicate that, in the latter cases, the resolution parameter κ is expected to be larger than under He implantation conditions

	Implantation	Fission reactor	Fusion reactor	Spallation source
Displacement rate (dpa/s)	1.5×10^{-6}	10^{-6}	10^{-6}	2×10^{-6}
He production rate (pa[a]/s)	1.5×10^{-8}	2×10^{-13}	6×10^{-12}	3×10^{-10}
He/dpa	10^{-2}	2×10^{-7}	6×10^{-6}	1.5×10^{-4}
$(P^{(1)2}/K^4)^{1/7}$ ($s^{2/7}$)	12.4	0.63	1.67	3.4
Critical He conc. (%)	1	$\leqslant 5\times10^{-2}$	$\leqslant 0.135$	$\leqslant 0.27$
Critical dose (dpa)	1	$\leqslant 2500$	$\leqslant 225$	$\leqslant 18.4$

[a] pa: per matrix atom.

model' to the hardening of steels due to He implanted at or somewhat above room temperature (somewhat below or around $0.2T_m$), would formally require values for the 'obstacle strength' of sub-nm scale bubbles formed at such temperatures (numerical factor missing in Eq. (7)) much lower (<0.1) than commonly assumed (≈ 0.2 [21]), and is therefore doubtful. More experimental and theoretical work is required to clarify this problem.

5. Summary and perspectives

Many TEM observations of bubble structures formed in metals and alloys during He ion implantation or during irradiation associated with He production at intermediate temperatures ($0.2T_m < T < 0.5T_m$) show clearly that displacement cascades result in the resolution of He atoms from existing bubbles, inducing the nucleation of later generations of bubbles at displacement doses above about 0.1 dpa. In the present contribution, this phenomenon and its implications for hardening and embrittlement has been discussed.

A simple model allowing a fully analytical description of both the gas resolution from existing bubbles by displacement cascades and the nucleation of bubbles under the related internal He generation has been presented. For this, it has been assumed that a certain fraction of He atoms in a bubble (characterised by a resolution parameter) is resolved per dpa and that di-He clusters form immobile stable bubble nuclei. These assumptions have been shown to yield a linear increase of the bubble density with dose at constant average bubble size, in qualitative and crude quantitative agreement with experimental data.

In principle, already intra-cascade reactions of the debris of one primary bubble hit by a cascade may yield several stable secondary bubbles which would result in a higher bubble density and a lower average bubble size than predicted by the present simple model. On the other hand, the possibility of inter-cascade migration and coalescence of small bubbles is expected to result in a reduction of the bubble density and an increase of the bubble size compared to the values predicted by the present model. Both effects would have to be included in a more sophisticated future model of bubble formation at high dose levels.

The use of the present simple model for bubble formation under cascade damage conditions within the framework of the 'dispersed barrier hardening model' predicts a change from an initially very weak increase of the contribution of bubbles to hardening with increasing He concentration/dose to a significantly stronger dependence at higher doses. This result of the model provides an explanation for the transition form a displacement damage dominated hardening at low doses/He concentrations (<1 at.%/1 dpa) to a He dominated hardening at higher doses as found in systematic mechanical tests on austenitic and martensitic steels implanted with He at or somewhat above room temperature. In the present paper, this change is found to occur at a 'critical He concentration'/'critical dose' depending on the He-to dpa-ratio, which provides a basis for extrapolating the data for mechanical tests after He implantation to irradiation conditions of fast fission reactors, fusion reactors, and spallation neutron sources.

The trends in hardening predicted by the present model should be systematically checked by mechanical tests on samples implanted with He to different concentration levels between 0.05 and about 1 at.% and irradiated (simultaneously) with self-ions or (subsequently) with fast neutrons up to displacement doses of several dpa. In future attempts to quantitatively model hardening due to He, implanted or produced at low to intermediate temperatures a detailed theoretical study of the 'obstacle strength' of sub-nm scale bubbles formed at such temperatures would have to be included, in addition to a more sophisticated model of He cluster and bubble formation.

References

[1] H. Ullmaier, Nucl. Fusion 24 (1984) 1039.
[2] H. Ullmaier, J. Nucl. Mater. 133&134 (1985) 100.
[3] H. Trinkaus, J. Nucl. Mater. 133&134 (1985) 105.
[4] H. Ullmaier, E. Camus, J. Nucl. Mater. 251 (1997) 100.
[5] J.D. Hunn, E.H. Lee, T.S. Byun, L.K. Mansur, J. Nucl. Mater. 282 (2000) 131.
[6] E.H. Lee, T.S. Byun, J.D. Hunn, K. Farrell, L.K. Mansur, J. Nucl. Mater. 296 (2001) 183.
[7] H. Ullmaier, J. Chen, these Proceedings. doi:10.1016/S0022-3115(03)00024-2.
[8] H. Trinkaus, J. Nucl. Mater. 118 (1983) 39.
[9] B.N. Singh, H. Trinkaus, J. Nucl. Mater. 186 (1991) 153.
[10] R.S. Nelson, J. Nucl. Mater. 31 (1969) 153.
[11] P. Chou, N.M. Ghoniem, J. Nucl. Mater. 117 (1983) 55.
[12] P. Chou, N.M. Ghoniem, Nucl. Instrum. and Meth. B 9 (1985) 209.
[13] N.M. Ghoniem, J. Nucl. Mater. 174 (1990) 168.
[14] P. Dauben, R.P. Wahi, H. Wollenberger, J. Nucl. Mater. 141–143 (1986) 723.
[15] N. Wanderka, E. Camus, H. Wollenberger, unpublished work (1996).
[16] H. Trinkaus, in preparation for publication.
[17] S.J. Kim, M.A. Nicolet, R.S. Averback, D. Peak, Phys. Rev. B 37 (1988) 38.
[18] D. Schwahn, H. Ullmaier, J. Schelten, W. Kesternich, Acta Mater. 31 (1983) 2003.
[19] G.W. Greenwood, A.J.E. Foreman, E.A. Rimmer, J. Nucl. Mater. 4 (1959) 305.
[20] N.M. Ghoniem, S. Sharafat, J.M. Williams, L.K. Mansur, J. Nucl. Mater. 117 (1983) 96.
[21] G.E. Lucas, J. Nucl. Mater. 206 (1993) 287.